Stimulated Raman scattering microscope with shot noise limited sensitivity using subharmonically synchronized laser pulses

Yasuyuki Ozeki,[1*, 2] Yuma Kitagawa,[1] Kazuhiko Sumimura,[1] Norihiko Nishizawa,[1] Wataru Umemura,[1] Shin'ichiro Kajiyama,[4] Kiichi Fukui,[3] and Kazuyoshi Itoh[1]

[1]Department of Material and Life Science, Graduate School of Engineering, Osaka University, 2-1 Yamadaoka, Suita, Osaka 565-0871, Japan
[2]PRESTO, Japan Science and Technology Agency (JST), 4-1-8 Honcho, Kawaguchi, Saitama 332-0012, Japan
[3]Department of Biotechnology, Graduate School of Engineering, Osaka University, 2-1 Yamadaoka, Suita, Osaka 565-0871, Japan
[4]School of Biology-Oriented Science and Technology, Kinki University, Osaka, Japan
**ozeki@mls.eng.osaka-u.ac.jp*

Abstract: We propose and demonstrate the use of subharmonically synchronized laser pulses for low-noise lock-in detection in stimulated Raman scattering (SRS) microscopy. In the experiment, Yb-fiber laser pulses at a repetition rate of 38 MHz are successfully synchronized to Ti:sapphire laser pulses at a repetition rate of 76 MHz with a jitter of <8 fs by a two-photon detector and an intra-cavity electro-optic modulator. By using these pulses, high-frequency lock-in detection of SRS signal is accomplished without high-speed optical modulation. The noise level of the lock-in signal is found to be higher than the shot noise limit only by 1.6 dB. We also demonstrate high-contrast, 3D imaging of unlabeled living cells.

OCIS codes: (320.7090) Ultrafast lasers; (180.5655) Raman microscopy

References and links

1. Y. Barad, H. Eisenberg, M. Horowitz, and Y. Silberberg, "Nonlinear scanning laser microscopy by third harmonic generation," Appl. Phys. Lett. **70**(8), 922–924 (1997).
2. P. J. Campagnola, M.-D. Wei, A. Lewis, and L. M. Loew, "High-resolution nonlinear optical imaging of live cells by second harmonic generation," Biophys. J. **77**(6), 3341–3349 (1999).
3. A. Zumbusch, G. R. Holtom, and X. S. Xie, "Three-dimensional vibrational imaging by coherent anti-Stokes Raman scattering," Phys. Rev. Lett. **82**(20), 4142–4145 (1999).
4. M. Hashimoto, T. Araki, and S. Kawata, "Molecular vibration imaging in the fingerprint region by use of coherent anti-Stokes Raman scattering microscopy with a collinear configuration," Opt. Lett. **25**(24), 1768–1770 (2000), http://www.opticsinfobase.org/ol/abstract.cfm?URI=ol-25-24-1768.
5. K. Isobe, S. Kataoka, R. Murase, W. Watanabe, T. Higashi, S. Kawakami, S. Matsunaga, K. Fukui, and K. Itoh, "Stimulated parametric emission microscopy," Opt. Express **14**(2), 786–793 (2006), http://www.opticsinfobase.org/oe/abstract.cfm?URI=oe-14-2-786.
6. D. Fu, T. Ye, T. E. Matthews, G. Yurtsever, and W. S. Warren, "Two-color, two-photon, and excited-state absorption microscopy," J. Biomed. Opt. **12**(5), 054004 (2007).
7. C. W. Freudiger, W. Min, B. G. Saar, S. Lu, G. R. Holtom, C. He, J. C. Tsai, J. X. Kang, and X. S. Xie, "Label-free biomedical imaging with high sensitivity by stimulated Raman scattering microscopy," Science **322**(5909), 1857–1861 (2008).
8. Y. Ozeki, F. Dake, S. Kajiyama, K. Fukui, and K. Itoh, "Analysis and experimental assessment of the sensitivity of stimulated Raman scattering microscopy," Opt. Express **17**(5), 3651–3658 (2009), http://www.opticsinfobase.org/oe/abstract.cfm?URI=oe-17-5-3651.
9. P. Nandakumar, A. Kovalev, and A. Volkmer, "Vibrational imaging based on stimulated Raman scattering microscopy," N. J. Phys. **11**(3), 033026 (2009).
10. W. Min, S. Lu, S. Chong, R. Roy, G. R. Holtom, and X. S. Xie, "Imaging chromophores with undetectable fluorescence by stimulated emission microscopy," Nature **461**(7267), 1105–1109 (2009).
11. A. Volkmer, J.-X. Cheng, and X. S. Xie, "Vibrational imaging with high sensitivity via epidetected coherent anti-Stokes Raman scattering microscopy," Phys. Rev. Lett. **87**(2), 023901 (2001).
12. J.-X. Cheng, L. D. Book, and X. Sunney Xie, "Polarization coherent anti-Stokes Raman scattering microscopy," Opt. Lett. **26**(17), 1341–1343 (2001), http://www.opticsinfobase.org/ol/abstract.cfm?URI=ol-26-17-1341.

#128225 - $15.00 USD Received 10 May 2010; revised 3 Jun 2010; accepted 6 Jun 2010; published 10 Jun 2010

13. C. L. Evans, E. O. Potma, and X. S. Xie, "Coherent anti-stokes raman scattering spectral interferometry: determination of the real and imaginary components of nonlinear susceptibility $\chi^{(3)}$ for vibrational microscopy," Opt. Lett. **29**(24), 2923–2925 (2004), http://www.opticsinfobase.org/ol/abstract.cfm?URI=ol-29-24-2923.
14. F. Ganikhanov, C. L. Evans, B. G. Saar, and X. S. Xie, "High-sensitivity vibrational imaging with frequency modulation coherent anti-Stokes Raman scattering (FM CARS) microscopy," Opt. Lett. **31**(12), 1872–1874 (2006), http://www.opticsinfobase.org/ol/abstract.cfm?URI=ol-31-12-1872.
15. H. Kano, and H. O. Hamaguchi, "Vibrationally resonant imaging of a single living cell by supercontinuum-based multiplex coherent anti-Stokes Raman scattering microspectroscopy," Opt. Express **13**(4), 1322–1327 (2005), http://www.opticsinfobase.org/oe/abstract.cfm?URI=oe-13-4-1322.
16. Y. Ozeki, and K. Itoh, "Stimulated Raman scattering microscopy for live-cell imaging with high contrast and high sensitivity," Laser Phys. **20**(5), 1114–1118 (2010).
17. C. L. Evans, E. O. Potma, M. Puoris'haag, D. Côté, C. P. Lin, and X. S. Xie, "Chemical imaging of tissue in vivo with video-rate coherent anti-Stokes Raman scattering microscopy," Proc. Natl. Acad. Sci. U.S.A. **102**(46), 16807–16812 (2005).
18. C. Heinrich, A. Hofer, A. Ritsch, C. Ciardi, S. Bernet, and M. Ritsch-Marte, "Selective imaging of saturated and unsaturated lipids by wide-field CARS-microscopy," Opt. Express **16**(4), 2699–2708 (2008), http://www.opticsinfobase.org/oe/abstract.cfm?URI=oe-16-4-2699.
19. T. Minamikawa, M. Hashimoto, K. Fujita, S. Kawata, and T. Araki, "Multi-focus excitation coherent anti-Stokes Raman scattering (CARS) microscopy and its applications for real-time imaging," Opt. Express **17**(12), 9526–9536 (2009), http://www.opticsinfobase.org/oe/abstract.cfm?URI=oe-17-12-9526.
20. B. F. Levine, C. V. Shank, and J. P. Heritage, "Surface vibrational spectroscopy using stimulated Raman scattering," IEEE J. Quantum Electron. **15**(12), 1418–1432 (1979).
21. B. G. Saar, G. R. Holtom, C. W. Freudiger, C. Ackermann, W. Hill, and X. S. Xie, "Intracavity wavelength modulation of an optical parametric oscillator for coherent Raman microscopy," Opt. Express **17**(15), 12532–12539 (2009), http://www.opticsinfobase.org/oe/abstract.cfm?URI=oe-17-15-12532.
22. D. D. Hudson, K. W. Holman, R. J. Jones, S. T. Cundiff, J. Ye, and D. J. Jones, "Mode-locked fiber laser frequency-controlled with an intracavity electro-optic modulator," Opt. Lett. **30**(21), 2948–2950 (2005), http://www.opticsinfobase.org/ol/abstract.cfm?URI=ol-30-21-2948.
23. R. Salem, and T. E. Murphy, "Broad-band optical clock recovery system using two-photon absorption," IEEE Photon. Technol. Lett. **16**(9), 2141–2143 (2004).
24. T. Minamikawa, N. Tanimito, M. Hashimoto, T. Araki, M. Kobayashi, K. Fujita, and S. Kawata, "Jitter reduction of two synchronized picosecond mode-locked lasers using balanced cross-correlator with two-photon detectors," Appl. Phys. Lett. **89**(19), 191101 (2006).
25. S. Takasaka, Y. Ozeki, S. Namiki, and M. Sakano, "External synchronization of 160-GHz optical beat signal by optical phase-locked loop technique," IEEE Photon. Technol. Lett. **18**(23), 2457–2459 (2006).
26. Y. Kobayashi, X. Zhou, D. Yoshitomi, and K. Torizuka, "Passive timing synchronization between Ti:sapphire laser and Yb-doped fiber laser," in Conference on Lasers and Electro-Optics/Quantum Electronics and Laser Science Conference and Photonic Applications Systems Technologies, OSA Technical Digest (CD) (Optical Society of America, 2008), paper CML6. *http://www.opticsinfobase.org/abstract.cfm?URI=CLEO-2008-CML6*.
27. R. K. Shelton, S. M. Foreman, L.-S. Ma, J. L. Hall, H. C. Kapteyn, M. M. Murnane, M. Notcutt, and J. Ye, "Subfemtosecond timing jitter between two independent, actively synchronized, mode-locked lasers," Opt. Lett. **27**(5), 312–314 (2002), http://www.opticsinfobase.org/ol/abstract.cfm?URI=ol-27-5-312.
28. T. R. Schibli, J. Kim, O. Kuzucu, J. T. Gopinath, S. N. Tandon, G. S. Petrich, L. A. Kolodziejski, J. G. Fujimoto, E. P. Ippen, and F. X. Kaertner, "Attosecond active synchronization of passively mode-locked lasers by balanced cross correlation," Opt. Lett. **28**(11), 947–949 (2003), http://www.opticsinfobase.org/ol/abstract.cfm?URI=ol-28-11-947.
29. D. J. Jones, E. O. Potma, J.-X. Cheng, B. Burfeindt, Y. Pang, J. Ye, and X. S. Xie, "Synchronization of two passively mode-locked, picosecond lasers within 20 fs for coherent anti-Stokes Raman scattering microscopy," Rev. Sci. Instrum. **73**(8), 2843–2848 (2002).
30. F. Ganikhanov, S. Carrasco, X. Sunney Xie, M. Katz, W. Seitz, and D. Kopf, "Broadly tunable dual-wavelength light source for coherent anti-Stokes Raman scattering microscopy," Opt. Lett. **31**(9), 1292–1294 (2006), http://www.opticsinfobase.org/ol/abstract.cfm?URI=ol-31-9-1292.
31. K. Kieu, B. G. Saar, G. R. Holtom, X. S. Xie, and F. W. Wise, "High-power picosecond fiber source for coherent Raman microscopy," Opt. Lett. **34**(13), 2051–2053 (2009), http://www.opticsinfobase.org/ol/abstract.cfm?URI=ol-34-13-2051.

1. Introduction

Various types of coherent nonlinear-optical microscopy techniques [1–10] have been demonstrated for label-free, 3-dimensional observation of biological samples. In particular, lock-in detection technique introduced recently allows us to employ novel contrast mechanisms such as two-photon absorption [6], excited state absorption [6], stimulated Raman scattering (SRS) [7–9] and stimulated emission [10]. A common advantage of these contrast mechanisms is that they give us background-free images with high sensitivity. Indeed, SRS microscopy provides high vibrational contrast without nonresonant background, which has been a crucial issue to be solved in coherent anti-Stokes Raman scattering (CARS)

#128225 - $15.00 USD Received 10 May 2010; revised 3 Jun 2010; accepted 6 Jun 2010; published 10 Jun 2010

microscopy [3,4,11–15]. Furthermore, the sensitivity of SRS microscopy at the shot noise limit is comparable to CARS microscopy [8]. The sensitivity merit of SRS and CARS over the spontaneous Raman scattering is as much as 3 orders of magnitude or higher [16], and high-speed CARS microscopy operating at up to the video rate has been demonstrated [17–19].

In SRS microscopy, two-color laser pulses from pulsed laser oscillators are focused on a sample, and energy transfer between the pulses due to SRS is detected with the lock-in technique in the MHz frequency regime, as shown in Fig. 1(a). The use of such a high frequency, which was originally introduced in SRS spectroscopy [20], is important for distinguishing SRS signal from the laser intensity noise, which has huge 1/*f* noise over the white shot noise. Although the sensitivities of SRS spectroscopy and SRS microscopy have been reported to be near the shot noise limit [20,7,8], further increase of the lock-in frequency seems still advantageous because it pushes the sensitivity to the shot noise limit, and allows us to reduce the pixel dwell time for high-speed imaging in the future.

In previous SRS microscopy and spectroscopy, electro-optic and acousto-optic modulators have been used at the output of the pulse source [7–9,20] or in the cavity [21]. However, the introduction of these modulators based on free-space optics possibly leads to optical loss and/or complexity in electronics especially at such high modulation frequency. Here, considering that the maximum lock-in frequency is a half of the repetition frequency of the pulses [21], it seems straightforward to employ subharmonically synchronized two-color pulse trains, one of which has just a half of the repetition frequency of the other, as shown in Fig. 1(b). This configuration allows us to omit optical modulation while SRS signal could be detected at the maximum lock-in frequency. It would be beneficial if we could realize such a pulse source in a simple and stable setup. Note that the maximum lock-in frequency itself was already realized in SRS microscopy with a sophisticated optical parametric oscillator (OPO) with an intracavity wavelength modulator [21].

In this paper, we present a low-noise implementation of SRS microscopy by using the subharmonically synchronized laser sources. This paper is organized as follows. In section 2, we demonstrate the subharmonic synchronization of an Yb-fiber oscillator (YbF) to a Ti:sapphire oscillator (TiS) using a two-photon photodiode and an intra-cavity phase modulator. In Section 3, an SRS microscope is constructed and its noise level is confirmed to be close to the shot noise limit. We also demonstrate label-free SRS imaging of living cells. Section 4 discusses on the demonstrated technique. Section 5 summarizes this paper.

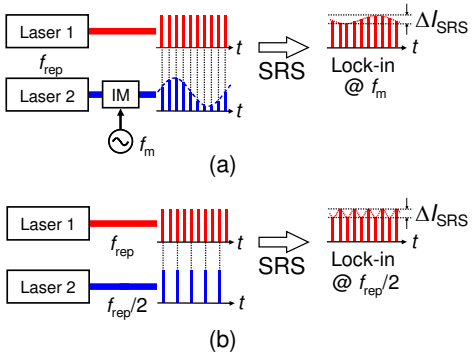

Fig. 1. Principle of lock-in detection of SRS signal employing (a) an intensity modulator (IM) and (b) subharmonically synchronized pulse sources demonstrated in this paper.

2. Active, subharmonic synchronization of two-color laser pulses

Figure 2 shows the schematic of the experimental setup. A TiS (Coherent, Mira 900F) generated a 76-MHz train of optical pulses at a wavelength of ~790 nm with a spectral width of 8 nm. The pulses were chirped with a glass block to expand the pulse duration to ~300 fs.

#128225 - $15.00 USD Received 10 May 2010; revised 3 Jun 2010; accepted 6 Jun 2010; published 10 Jun 2010

A home-made YbF, which was mode-locked by nonlinear polarization rotation, produced a 38-MHz train of chirped ~300-fs pulses at a wavelength of 1028 nm with a spectral width of 15 nm. In the cavity of YbF, an in-line phase modulator (PM) (Photline, NIR-MPX-LN-0.1) was inserted for high-speed control of the cavity length [22]. Since the half-wave voltage of the PM was as low as 2.3 V, we could use low-voltage circuits for driving the PM. A piezo-electric stage was also placed for low-speed, long-range adjustment of the cavity length by up to 300 µm. To detect the relative delay of the two-color pulses, portions of the pulses were tapped with polarization beam splitters, combined with a dichroic mirror, and collinearly focused on a GaAsP photodiode (PD) (Hamamatsu, G1115) with an objective lens (50x, NA0.55). The optical power was approximately 3 mW for each color. The two-photon absorption photocurrent produced by the PD gives the intensity cross correlation between the TiS and YbF pulses [23–25]. The PD signal was amplified with an electrical bandwidth of ~600 kHz. After the subtraction of the offset voltage, the PD signal was used as an error signal and was fed back to YbF through a loop filter, where proportional and integral control was employed. The remaining optical pulses were also combined after the adjustment of the delay, and were used for out-of-loop jitter measurement using another GaAsP photodiode or for SRS microscopy.

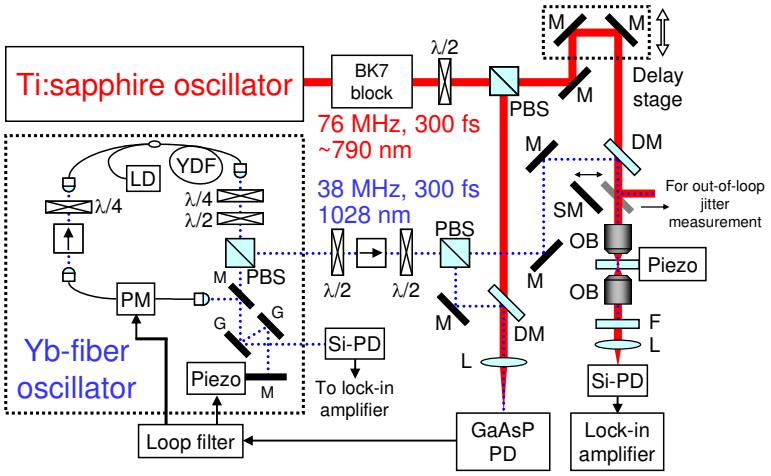

Fig. 2. Experimental setup. M: mirror, DM: dichroic mirror, SM: switchable mirror, PBS: polarization beam splitter, YDF: Yb-doped fiber, G: diffraction grating, LD: 980-nm pump laser diode, PM: in-line phase modulator, PD: photodiode, L: lens, OB: objective lens, F: short-pass filter.

Before the synchronization experiment, we measured the two-photon signal as a function of the relative delay. This was accomplished under the free-running condition by observing the in-loop GaAsP PD signal with an oscilloscope, which was triggered by the out-of-loop GaAsP PD signal. The horizontal axis was calibrated by introducing a path length difference of 3 mm, which corresponds to a relative delay of 10 ps. As shown in Fig. 3(a), the in-loop two-photon signal increased when the two-color pulses were overlapped with each other. The curve has a slope of 6.0 V/ps around the zero-crossing point.

Figure 3(b) shows the waveform of the error signal measured when we closed the loop. First the loop was under the proportional control. Then the cavity length was adjusted by applying a driving voltage on the piezo stage. After the lasers were locked, the integral control was turned on to achieve tight locking.

Figures 3(c) and 3(d) show the error signal and its spectral density, respectively. The in-loop jitter and out-of-loop jitter were found to be 4.0 fs and 7.8 fs, respectively. The loop bandwidth was approximately 140 kHz. The limiting factor of the loop bandwidth is not clear at the moment. In order to investigate the origin of the increase in the out-of-loop jitter, the long-term (~50 s) fluctuation of the unlocked, in-loop two-photon signal was separately

#128225 - $15.00 USD Received 10 May 2010; revised 3 Jun 2010; accepted 6 Jun 2010; published 10 Jun 2010

measured (not shown) to be 40 mV, which corresponds to an additional jitter of 6.6 fs. Thus the total jitter is estimated to be 7.7 fs, which is in reasonable agreement with the out-of-loop jitter. The limiting factor of the achievable jitter in this experiment is the fluctuation of two-photon signal, which originates from the intensity jitter of the pulses. Such a jitter could be compensated for by employing a balanced cross-correlator using two GaAsP PD's [24]. We also measured the long-term timing jitter for 30 minutes. As shown in Fig. 3(e), the amount of timing drift is <10 fs within a bandwidth of 100 Hz. Compared to the previous report [26] which demonstrated the passive synchronization of Ti:S and YbF with a jitter of 3.2 fs in a bandwidth of 10 kHz, the active synchronization presented here is advantageous for obtaining long-term stability, as will be discussed in Section 4.1.

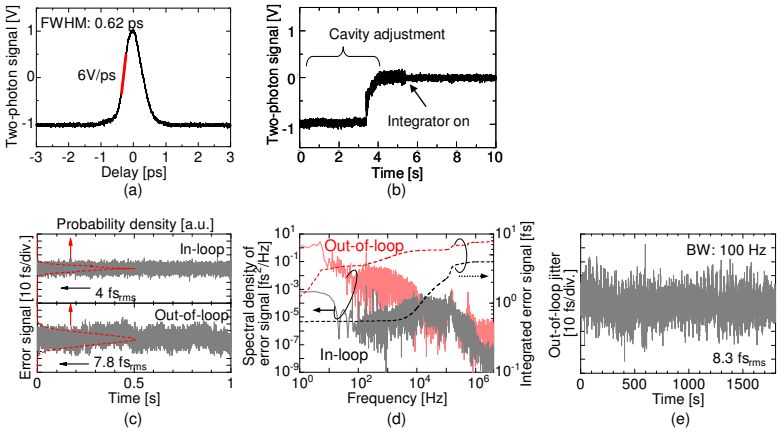

Fig. 3. Results of the synchronization experiment. (a) Intensity cross-correlation measured by the GaAsP PD. (b) The waveform of the error signal measured when the loop was closed. (c) Solid line: in-loop error signal (upper) and out-of-loop error signal (lower). Red broken line: probability densities. (d) Solid line: spectral densities of the in-loop (gray) and out-of-loop (red) error signals. Broken line: integrated jitter. (e) Long-term out-of-loop jitter measured for 30 min.

3. SRS microscopy experiment

3.1 Experimental setup

By using the synchronized pulse sources, an SRS microscope was constructed. As shown in Fig. 2, the synchronized pulses were focused on a sample with an objective lens (100x, NA1.4, oil). The position of the sample was scanned with a 3-axis piezoelectric transducer stage (PI, P-611.3S). The transmitted pulses were collected with another lens (100x, NA1.4, oil). After rejecting YbF pulses with an optical filter, TiS pulses were detected by a Si-PD. We used two kinds of Si-PD's: (i) a 45-MHz PD (Hamamatsu, S3072) with a transimpedance amplifier with a feedback resistance of 510 Ω, and (ii) a 100-MHz PD (Hamamatsu, S3399) terminated with a 510 Ω load resistor and an inductor, which compensates for the high junction capacitance of the PD at the lock-in frequency (i.e. 38 MHz). Both circuits showed comparable noise performance, but the latter exhibited slightly higher tolerance to the saturation of the electronic amplifier. The photocurrent was band-pass filtered, amplified and led to a high-frequency lock-in amplifier (Stanford research systems, SR844) to detect SRS signal. The reference signal at 38 MHz for the lock-in amplifier was obtained through the photodetection of YbF pulses tapped as the 0th diffraction from the grating compressor in the YbF cavity. In this paper, almost all the experiments were conducted with PD (i), whereas the noise level was measured with PD (ii).

#128225 - $15.00 USD Received 10 May 2010; revised 3 Jun 2010; accepted 6 Jun 2010; published 10 Jun 2010

3.2 Detection of SRS signal from a polystyrene bead

We measured the SRS spectrum of a polystyrene bead with a diameter of 10 μm. The optical powers of TiS and YbF pulses were set to ~3 mW and ~2 mW, respectively. It was possible to tune the wavelength of TiS without losing the lock although a slight adjustment of the offset voltage of the two-photon signal was necessary. The measurement of each point took ~10 s. The measured spectrum shown in Fig. 4(a) clearly confirms the aromatic CH stretching mode at 3050 cm^{-1}. The spectral resolution is approximately 100 cm^{-1}, which is limited by the duration of laser pulses (~300 fs) and seems to be still insufficient for high spectral resolution imaging. The spectral resolution would be improved by using picosecond pulses or by introducing a frequency chirp with dispersive components.

3.3 Evaluation of the noise level

We investigated the noise level of the lock-in voltage by changing the optical power incident on the PD. The result is shown in Fig. 4(b). We can see that the Johnson noise is dominant when the photocurrent is low, whereas the noise increases as the photocurrent increases. We plotted the shot noise level given by

$$v_{\mathrm{shot}} = RG\sqrt{\frac{2qi}{\tau}}, \tag{1}$$

where $R = 510\ \Omega$ is the load resistance, $G = 7.4$ is the gain of the amplifier, q is the elementary charge, i is the photocurrent, and $\tau = 0.1$ ms is the integration time of the lock-in amplifier. We note here that the factor of $2^{1/2}$ is the result of the fact that the lock-in frequency is just a half of the repetition frequency of the pulse. The details of this point will be discussed in Section 4.2. Figure 4(b) shows that the noise level is close to the shot noise limit by 1.6 dB for $i > 0.2$ mA. The discrepancy between the experimental and theoretical shot noises is probably due to the insufficient optimization of bandpass filters employed in the photodetection circuit. Nevertheless, the noise level of the current system is very close to the shot noise limit.

The PD circuit was saturated at a photocurrent of >3 mW, which corresponds to the optical intensity of ~5 mW at the PD input. The saturation seems to be caused by the electric amplifier due to the strong photocurrent at 76 MHz. Further optimization of the PD circuit will improve the saturation intensity. We investigated the saturation characteristics of the PD itself at a frequency of 38 MHz and found that the saturation intensity is approximately 15 mW, which seems enough for biological imaging applications.

The present noise level can be compared with our previous result, where the lock-in frequency was set to 10.7 MHz and the voltage noise of lock-in signal was 12.8 μV for i = 0.25 mA, τ = 5 ms, G = 18, and R = 1.1 kΩ [8]. Considering that the noise level is proportional to $RG/\tau^{1/2}$, the previous noise level, which was dominated by laser intensity noise, corresponds to 17.3 μV in the present experimental condition, which is shown by a cross in Fig. 4(b). It can be seen that we could drastically reduce the noise level by >12 dB, which is attributed to the increase of lock-in frequency.

#128225 - $15.00 USD Received 10 May 2010; revised 3 Jun 2010; accepted 6 Jun 2010; published 10 Jun 2010

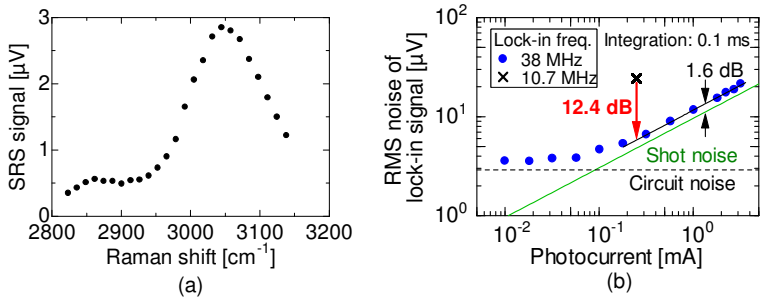

Fig. 4. (a) SRS spectrum of a polystyrene bead with a diameter of 10 μm. (b) Circle: noise level of the lock-in signal as a function of photocurrent of Si-PD. Cross: corresponding noise level in our previous setup. Green line: theoretical shot noise level given by Eq. (1). Broken line: circuit noise.

3.4 SRS imaging

We observed a living tobacco BY-2 cell with the SRS microsope. The Raman shift was set to be 2850 cm^{-1} so that we can detect the CH_2 stretching mode. The average powers of TiS and YbF pulses at the focus were set to be as low as 2.0 mW and 1.3 mW, respectively. The pixel dwell time was set to 0.2 ms. As shown in Fig. 5(a) (Media 1), we could clearly visualize cellular components such as a nucleus, cell wall and vacuoles as well as small droplets which are likely assigned to mitochondria [3].

Next we observed a cultured HeLa cell. The Raman shift was the same as the above experiment. The average powers of TiS and YbF pulses at the focus were set to be 1.9 mW for each. The pixel dwell time was set to 0.5 ms. As shown in Fig. 5(b) (Media 2), the distribution of several droplets possibly due to the lipids were clearly visualized in 3D. The high-contrast nature of SRS microscopy is evident from these images.

Note that the pixel dwell time in this experiment is limited by several factors such as response time of the piezo actuator for sample scanning, the optical power of YbF, and the bandwidth of lock-in amplifier. Nevertheless, they are not essential limitation of SRS microscopy.

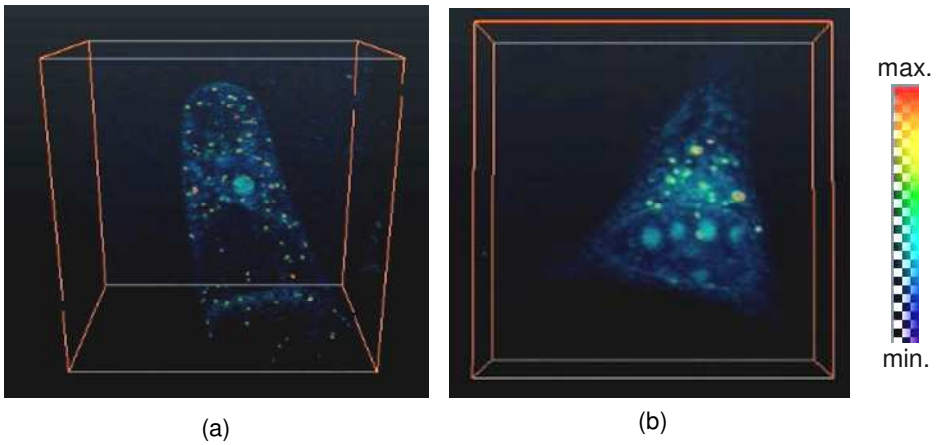

Fig. 5. 3D SRS images of (a) a cultured tobacco BY-2 cell (Media 1), and (b) a cultured HeLa cell (Media 2). The pixel dwell time: (a) 0.2 ms, (b) 0.5 ms. Number of pixels: (a) 300 x 300 x 40, (b) 400 x 400 x 32. The size of the observed region: (a) 60 x 60 x 40 μm^3, (b) 40 x 40 x 10 μm^3.

#128225 - $15.00 USD Received 10 May 2010; revised 3 Jun 2010; accepted 6 Jun 2010; published 10 Jun 2010

4. Discussions

4.1 Effectiveness of active, wideband synchronization

Here we discuss the advantages of the presented synchronization technique compared to previous ones [24,26–29] considering jitter performance, long-term stability, and pull-in range. Our technique is characterized by (a) the active synchronization, (b) the use of all-optical phase detector, and (c) the wide loop bandwidth of >100 kHz.

In terms of the jitter, passive synchronization [26] is basically advantageous because the equivalent loop bandwidth can be easily widened by increasing the optical power of the master laser pulse launched to the slave laser. This point can be understood by considering that the loop characteristics of the injection locking are the same as a phase-locked loop under proportional control, and that there is no component which restricts the loop bandwidth in the passive synchronization. In active synchronization, the speed of cavity length control is the crucial factor that limits the loop bandwidth as well as the jitter performance. Indeed, when we used a high-speed piezo transducer to control the cavity length, the loop bandwidth was limited within ~1 kHz, resulting in the jitter of as much as ~2 ps. Thus wideband control based on the high-speed, non-mechanical control of the cavity length by use of electro-optic modulator [22] is effective for low-jitter synchronization of two-color laser pulses.

As for the long-term stability, the active synchronization is advantageous because we can incorporate the integral control, which minimizes the error signal in the low-frequency regime, allowing us to compensate for the drifts of the system parameters such as the free-running frequencies. Indeed, the synchronization in the presented experiment was so stable that we could conduct imaging experiments for several hours. Needless to say, it is also possible to obtain long-term stability in passive synchronization as well by incorporating a stabilizer at the expense of additional complexity.

Another important issue is the pull-in range. All-optical phase detectors such as two-photon photodiode or second-harmonic generation crystal are advantageous for the precise detection of the delay difference between the pulses. However, the pull-in range is quite narrow therein because the phase detection is possible only when the pulses are overlapped in time. To cope with this issue, an additional electronic phase comparator was employed in active synchronization of solid-state lasers in previous reports [24,28], leading to additional complexity in the setup. In contrast, we were able to synchronize two lasers without using such an additional phase comparator, leading to significant simplification.

The pull-in range can be estimated in the following manner. Assuming that two lasers are not synchronized and have a frequency difference of Δf, the pulses overlap with each other for a duration of approximately $\Delta t/\Delta f\ T$, where Δt and T are the pulse duration and the period, respectively. To achieve the lock, this duration should be longer than the response time of the feedback loop $1/B$, where B is the bandwidth of the loop. Thus Δf should satisfy

$$\Delta f < B\Delta t/T, \tag{2}$$

which gives an estimate of the pull-in range. Assuming B = 140 kHz, Δt = 300 fs, and T = 12 ns, we obtain Δf < 3 Hz, which is much wider than the frequency stability of our lasers of ~1 Hz. Thus the wideband control presented in this paper is advantageous for realizing a wide pull-in range. Although we have to adjust the free-running frequency of the laser to achieve the lock, such adjustment will be implemented with a cheap electronics comprising of photodiodes and a frequency counter.

From the viewpoint of the light sources for coherent Raman microscopy, OPO pumped by a picosecond mode-locked laser [30,31] seems to be a powerful choice in terms of high average power, low jitter, wide wavelength tunability, and high spectral resolution. On the other hand, our technique is suitable for extending an existing multiphoton microscope using a TiS to SRS microscope by attaching a Yb fiber oscillator based on established technologies.

To summarize, the presented technique is a simple and practical method for achieving precise synchronization of two-color lasers with long-term stability, and will be useful for SRS microscopy.

#128225 - $15.00 USD Received 10 May 2010; revised 3 Jun 2010; accepted 6 Jun 2010; published 10 Jun 2010

4.2 Signal-to-noise ratio at the subharmonic frequency

When the lock-in frequency is just a half of the repetition frequency as demonstrated in the experiment, the shot noise limited sensitivity is higher by 3 dB and the circuit noise limited sensitivity is higher by 6 dB compared to the sinusoidal modulation at other frequencies. To clarify this point, we derive the expressions of the lock-in signals.

We denote the peak power of the pulses and its modulation by SRS as I and δI, the repetition rate as ω_{rep}, the period of the pulse train as $T = 2\pi/\omega_{rep}$, the lock-in frequency as ω_0 ($\leq \omega_{rep}/2$), and the integration time as τ. We define the effective pulse width Δt as the pulse energy divided by the peak power. If we neglect the shot noise, the output voltage of the PD, on which the pulses are impinged, is given by

$$v(t) = R\frac{\eta q}{h\nu}\sum_m \left\{ h(t-mT)\Delta t\left[I_0 - \frac{\delta I}{2}\left(1+\cos\omega_0 mT\right)\right]\right\}, \tag{3}$$

where t is the time, R is the load resistance, η is the quantum efficiency of the PD, q is the elementary charge, $h\nu$ is the photon energy, m is an integer, and $h(t)$ is the impulse response of the PD, which satisfies

$$\int h(t)\,\mathrm{d}t = 1. \tag{4}$$

The output voltage of the lock-in amplifier, which displays the rms voltage of $v(t)$, is defined as

$$v_{\mathrm{L}} = \frac{\sqrt{2}}{\tau}\int_0^\tau v(t')\cos\omega_0 t'\,\mathrm{d}t', \tag{5}$$

where we assume, without loss of generality, that the lock-in signal is averaged over $t = 0 \sim \tau$. Substituting Eq. (3) to Eq. (5) and assuming that $h(t)$ is nonzero only around $t \sim 0$, we obtain

$$\begin{aligned} v_{\mathrm{L}} &= \frac{\sqrt{2}}{\tau}\frac{R\eta q}{h\nu}\int_0^\tau \cos\omega_0 t'\sum_m \left\{ h(t'-mT)\Delta t\left[I_0 - \frac{\delta I}{2}\left(1+\cos\omega_0 mT\right)\right]\right\}\mathrm{d}t' \\ &= \frac{\sqrt{2}}{\tau}\frac{R\eta q}{h\nu}\int \cos\omega_0 t'\sum_{m=0}^{N-1}\left\{ h(t'-mT)\Delta t\left[I_0 - \frac{\delta I}{2}\left(1+\cos\omega_0 mT\right)\right]\right\} \\ &= \frac{\sqrt{2}R\eta q\Delta t}{h\nu\tau}\left[I_0 - \frac{\delta I}{2}\right]\sum_{m=0}^{N-1}\int h(t')\cos\omega_0(t'+mT)\,\mathrm{d}t' \\ &\quad - \frac{\sqrt{2}R\eta q\Delta t\delta I}{2h\nu\tau}\sum_{m=0}^{N-1}\int h(t')\cos\omega_0(t'+mT)\cos m\omega_0 T\,\mathrm{d}t', \end{aligned} \tag{6}$$

where $N = \tau/T$ is the number of pulses incoming in $0 \leq t < \tau$. If the averaging time is sufficiently long, the 1st term in the right hand side of Eq. (6) becomes

$$\begin{aligned} &\frac{\sqrt{2}R\eta q\Delta t}{h\nu\tau}\left[I_0 - \frac{\delta I}{2}\right]\sum_{m=0}^{N-1}\int h(t')\cos\omega_0(t'+mT)\,\mathrm{d}t' \\ &= \frac{\sqrt{2}R\eta q\Delta t}{h\nu\tau}\left[I_0 - \frac{\delta I}{2}\right]\sum_{m=0}^{N-1}\left[\cos m\omega_0 T\,\mathrm{Re}\,H(\omega_0) + \sin m\omega_0 T\,\mathrm{Im}\,H(\omega_0)\right] \\ &= 0, \end{aligned} \tag{7}$$

where Re and Im stand for the real and imaginary parts, respectively, and

$$H(\omega) = \int h(t)e^{-i\omega t}\,\mathrm{d}t \tag{8}$$

#128225 - $15.00 USD Received 10 May 2010; revised 3 Jun 2010; accepted 6 Jun 2010; published 10 Jun 2010

is the Fourier transform of $h(t)$. Thus Eq. (6) can be calculated as

$$\begin{aligned} v_{\mathrm{L}} &= -\frac{\sqrt{2}R\eta q\Delta t\delta I}{2h\nu\tau}\sum_{m=0}^{N-1}\int h(t')\cos\omega_0(t'+mT)\cos m\omega_0 T\,\mathrm{d}t' \\ &= -\frac{\sqrt{2}R\eta q\Delta t\delta I}{4\tau h\nu}\sum_{m=0}^{N-1}\left[\mathrm{Re}\,H(\omega)\cos 2mT+\mathrm{Im}\,H(\omega)\sin 2mT+\mathrm{Re}\,H(\omega)\right] \qquad (9) \\ &= \begin{cases} -\dfrac{\sqrt{2}R\eta q\Delta t\delta I}{2h\nu T}\mathrm{Re}\,H(\omega), & \omega_0=\dfrac{\omega_{\mathrm{rep}}}{2}, \\ -\dfrac{\sqrt{2}R\eta q\Delta t\delta I}{4h\nu T}\mathrm{Re}\,H(\omega), & 0<\omega_0<\dfrac{\omega_{\mathrm{rep}}}{2}, \end{cases} \end{aligned}$$

indicating that the lock-in signal is doubled at the subharmonic frequency. This signal gain is advantageous for improving the circuit-noise-limited SNR by 6 dB.

Next we calculate the shot noise in the lock-in signal. Since the index of intensity modulation due to SRS is typically small, its effect on the shot noise is negligible. Here we denote the fluctuation of the peak power of the m^{th} pulse as ΔI_m to obtain the deviation of the lock-in voltage Δv_{L} given by

$$\begin{aligned} \Delta v_{\mathrm{L}} &= \frac{\sqrt{2}R\eta q\Delta t}{h\nu\tau}\sum_{m=0}^{N-1}\Delta I_m\int h(t')\cos\omega_0(t'+mT)\,\mathrm{d}t' \\ &= \frac{\sqrt{2}R\eta q\Delta t}{h\nu\tau}\sum_{m=0}^{N-1}\Delta I_m\left[\mathrm{Re}\,H(\omega)\cos m\omega_0 T+\mathrm{Im}\,H(\omega)\sin m\omega_0 T\right]. \end{aligned} \qquad (10)$$

Therefore the variance of the lock-in voltage is

$$\begin{aligned} \overline{\Delta v_{\mathrm{L}}^2} &= \left[\frac{\sqrt{2}R\eta q\Delta t}{h\nu\tau}\right]^2\sum_{m=0}^{N-1}\Delta I_m^2\left\{\left[\mathrm{Re}\,H(\omega)\right]^2\cos^2 m\omega_0 T+\left[\mathrm{Im}\,H(\omega)\right]^2\sin^2 m\omega_0 T\right\} \\ &= \left[\frac{\sqrt{2}R\eta q\Delta t}{h\nu\tau}\right]^2\sum_{m=0}^{N-1}\Delta I_m^2\left\{\left[\mathrm{Re}\,H(\omega)\right]^2\frac{1+\cos 2m\omega_0 T}{2}+\left[\mathrm{Im}\,H(\omega)\right]^2\frac{1-\cos 2m\omega_0 T}{2}\right\} \qquad (11) \\ &= \begin{cases} \left[\dfrac{\sqrt{2}R\eta q\Delta t}{h\nu\tau}\right]^2\left[\mathrm{Re}\,H(\omega)\right]^2\displaystyle\sum_{m=0}^{N-1}\Delta I_m^2, & \omega_0=\dfrac{\omega_{\mathrm{rep}}}{2}, \\ \left[\dfrac{\sqrt{2}R\eta q\Delta t}{h\nu\tau}\right]^2\dfrac{\left|H(\omega)\right|^2}{2}\displaystyle\sum_{m=0}^{N-1}\Delta I_m^2, & 0<\omega_0<\dfrac{\omega_{\mathrm{rep}}}{2}. \end{cases} \end{aligned}$$

Here we estimate ΔI_m as follows. The number of the photocarriers generated by an optical pulse with a peak power of I_0 is given by $\eta\Delta tI_0/h\nu$. Due to the property of the Poissonian distribution, the number of photocarriers is equal to its variance. Therefore

$$\overline{\Delta I_{\mathrm{m}}^2}=\frac{h\nu I_0}{\eta\Delta t}. \qquad (12)$$

From Eqs. (11) and (12), we obtain the shot noise in the lock-in voltage as

#128225 - $15.00 USD Received 10 May 2010; revised 3 Jun 2010; accepted 6 Jun 2010; published 10 Jun 2010

$$\sqrt{\overline{\Delta v_{\mathrm{L}}^2}} = \begin{cases} Rq\sqrt{\dfrac{2\eta\Delta t I_0}{h\nu\tau T}}\left|\mathrm{Re}\,H(\omega)\right|, & \omega_0 = \dfrac{\omega_{\mathrm{rep}}}{2}, \\ Rq\sqrt{\dfrac{\eta\Delta t I_0}{h\nu\tau T}}\left|H(\omega)\right|, & 0 < \omega_0 < \dfrac{\omega_{\mathrm{rep}}}{2}. \end{cases} \tag{13}$$

From Eqs. (9) and (13), the signal-to-noise ratio (SNR) can be written as

$$\frac{v_{\mathrm{L}}^2}{\overline{\Delta v_{\mathrm{L}}^2}} = \begin{cases} \dfrac{\delta I^2 \eta \Delta t \tau}{4h\nu T I_0}, & \omega_0 = \dfrac{\omega_{\mathrm{rep}}}{2}, \\ \dfrac{\delta I^2 \eta \Delta t \tau}{8h\nu T I_0}\left|\dfrac{\mathrm{Re}\,H(\omega)}{H(\omega)}\right|^2, & 0 < \omega_0 < \dfrac{\omega_{\mathrm{rep}}}{2}. \end{cases} \tag{14}$$

Equation (14) means that SNR is improved by 3 dB when $\omega_0 = \omega_{\mathrm{rep}}/2$. Here the shot noise level can be expressed using the DC photocurrent $i_0 = \eta q \Delta t I_0 / h\nu T$ by

$$\sqrt{\overline{\Delta v_{\mathrm{L}}^2}} = \begin{cases} R\sqrt{\dfrac{2qi_0}{\tau}}\,\mathrm{Re}\,H(\omega) & \omega_0 = \dfrac{\omega_{\mathrm{rep}}}{2}, \\ R\sqrt{\dfrac{qi_0}{\tau}}\left|H(\omega)\right| & 0 < \omega_0 < \dfrac{\omega_{\mathrm{rep}}}{2}, \end{cases} \tag{15}$$

which gives Eq. (1), where the amplifier gain is considered as well. In this way, SNR and shot noise are found to be higher at $\omega_0 = \omega_{\mathrm{rep}}/2$.

Intuitively, the improvement of shot noise limited SNR can be understood by referring Fig. 1. When $\omega_0 < \omega_{\mathrm{rep}}/2$, the pulses are modulated with a sinusoidal waveform as shown in Fig. 1(a). Although SRS is completely turned on or off at the minima and maxima of the sinusoidal waveform, SRS is partially turned on or off between them. In contrast, when $\omega_0 = \omega_{\mathrm{rep}} / 2$, SRS is completely turned on or off for every optical pulse as shown in Fig. 1(b). This is the origin of the signal-to-noise merit of 3 dB. Note that we could have the same SNR merit by employing the rectangular modulation and rectangular lock-in detection. However, such a technique requires wideband modulation and photodetection, leading to additional complexity in the electronics. It is also noted that the theoretical sensitivity comparison between SRS and CARS in [8] is based on the rectangular modulation/detection.

The origin of the signal gain of 6 dB at $\omega_0 = \omega_{\mathrm{rep}}/2$ is explained as follows: The Fourier transform of the intensity waveform of an optical pulse train is composed of the DC component, the fundamental repetition rate (i.e. ω_0), and its harmonics. SRS modulates the intensity of the pulses, leading to the generation of sidebands at ω_0, $\omega_{\mathrm{rep}} - \omega_0$, $\omega_{\mathrm{rep}} + \omega_0$, etc. When $\omega_0 = \omega_{\mathrm{rep}}/2$, the first two sidebands interfere, giving the 6-dB gain. Thus it can be viewed as the result of aliasing effect.

The shot noise in the lock-in signal is also interesting at $\omega_0 = \omega_{\mathrm{rep}}/2$. When $\omega_0 \neq \omega_{\mathrm{rep}}/2$, there is no correlation between the arrival time of the pulses on the PD and the reference signal of the lock-in amplifier. Therefore shot noise is distributed to in-phase and out-of-phase lock-in signals. On the other hand, when $\omega_0 = \omega_{\mathrm{rep}}/2$, the arrival time is perfectly correlated to the reference signal. Therefore the shot noise is localized only in the in-phase component and enhanced by 3 dB. Note that the signal gain of 6 dB and the increase of shot noise by 3 dB are consistent with the SNR merit of 3 dB.

Thus the lock-in detection at the subharmonic frequency is advantageous not only for suppressing the 1/*f* laser intensity noise but also for pushing the shot noise limited SNR by 3 dB and the circuit-noise limited SNR by 6 dB.

#128225 - $15.00 USD Received 10 May 2010; revised 3 Jun 2010; accepted 6 Jun 2010; published 10 Jun 2010

5. Conclusion

We have demonstrated a high-sensitivity SRS microscope using subharmonically synchronized laser pulses. We achieved low-jitter (<8 fs), active, subharmonic synchronization of YbF to TiS by using a two-photon detector and an intra-cavity electro-optic modulator. By using the synchronized pulses, SRS signal was successfully detected and the noise level was measured to be close to the shot noise limit by 1.6 dB. We also demonstrated the label-free, 3D imaging of biological samples. The present synchronization technique is a simple and effective method for precise synchronization with long-term stability. The lock-in detection of SRS signal at the subharmonic frequency is advantageous for improving shot noise limited SNR by 3 dB and circuit noise limited SNR by 6 dB compared to other lock-in frequency. The presented technique can be applied to other microscopy techniques [6,10], and could be extended to a higher lock-in frequency simply by increasing the repetition rate of the oscillators.

Acknowledgments

The authors thank Makiko Ishii of Osaka University for the preparation of biological samples. K. I and Y. O thank Dr. H. Hashimoto and Dr. M. Hasegawa of Canon Co., Ltd. for their support on a part of this research.

#128225 - $15.00 USD Received 10 May 2010; revised 3 Jun 2010; accepted 6 Jun 2010; published 10 Jun 2010